Neurobiology of Disease 221 (2026) 107345

Contents lists available at ScienceDirect

Neurobiology of Disease

journal homepage: www.elsevier.com/locate/ynbdi

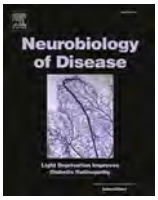

SGK1 inhibition restores excitability of cortical neurons derived from Alzheimer's disease patients

Zhongjiao Jiang, Komal Saleem, Emily Fisher, Li Li, Zhen Yan [*,1], Jian Feng [*,1]

Department of Physiology and Biophysics, State University of New York at Buffalo, Buffalo, NY 14203, United States

ARTICLE INFO

Keywords:
Alzheimer's disease
Induced pluripotent stem cells
Cortical neurons
SGK1
Neuronal excitability
Synaptic transmission

ABSTRACT

The vast majority of Alzheimer's disease (AD) cases are sporadic, without a clear etiology. We have previously found increased expression of Serum and Glucocorticoid-regulated Kinase 1 (SGK1) in mouse models of dementia, postmortem cortical tissues and induced pluripotent stem cells (iPSCs)-derived cortical neurons from patients with sporadic AD (sAD). SGK1 is induced by a variety of cellular stress. The physiological consequences of elevated SGK1 in sAD is unclear. Here, we differentiated iPSCs from four sAD patients and four age- and sex-matched healthy controls into electrophysiologically mature cortical neurons with prolonged culture for more than 100 days. The sAD cortical neurons exhibited significant reductions in voltage-gated Na^+ currents, amplitudes of evoked action potentials, and frequencies of spontaneous excitatory postsynaptic currents and spontaneous action potentials. Application of a selective inhibitor of SGK1 reversed all these phenotypes in sAD neurons without affecting control neurons. The SGK1-dependent hypoexcitability suggests that a convergent and inborn mechanism attenuates neuronal communications despite different genetic background of the sAD patients. Their iPSC-derived cortical neurons have captured the defective neurotransmission, which underlies cognitive and memory symptoms of AD, many decades before clinical manifestations. The study offers a new pathway to restore synaptic transmission in AD.

1. Introduction

Sporadic Alzheimer's disease (sAD), which has no clear inheritance pattern, accounts for more than 95% of AD cases (Masters et al., 2015). Despite the tremendous progress in understanding monogenic forms of AD, there are significant challenges in studying sAD beyond the common pathological hallmarks, such as Aβ and Tau, and the most prominent genetic risk factor ApoE4 (Rollo et al., 2023). Our previous study has identified increased expression of Serum- and Glucocorticoid-induced Kinase 1 (SGK1) in postmortem cortical tissue from sAD patients, P301S Tau transgenic mice, and 5 × FAD mice (Cao et al., 2020). Consistent with these, increased expression of SGK1 is observed in an independent single-cell RNA sequencing study of postmortem prefrontal cortical tissue from AD patients (Mathys et al., 2019). Increased expression of SGK1 appears to be critically involved in AD pathogenesis, as inhibition of SGK1 rescues the deficits in synaptic transmission and cognitive behavioral performance in the P301S Tau transgenic mouse model of dementia (Cao et al., 2020).

As a serine/threonine kinase responding to a variety of cellular stresses (Di Cristofano, 2017), SGK1 protein is not constitutively active but requires activation by phosphorylation, which is dependent on PI3K/PDK1 and mTOR signaling (Davoody et al., 2024; Lang et al., 2020). The kinase activity of SGK1 plays important roles in the regulation of ion channels, cell signaling, transcription, neuronal excitability, and cell death (Lang et al., 2018; Lang et al., 2010). SGK1 in the brain has been shown to be critical in spatial memory under physiological conditions (Chao et al., 2007), for example, expression of a dominant-negative mutant Sgk1 in the CA1 region of rat hippocampus significantly impairs water maze perform (Tsai et al., 2002). SGK1 upregulation has also been reported in a variety of neurodegenerative disorders involving cellular stress (Elahi et al., 2021,Kwon et al., 2021,Lian et al., 2020, Schoenebeck et al., 2005,Talarico et al., 2016), however, its pathological functions are largely unknown in human neurons.

Patient-specific iPSC-derived neurons have captured human-unique pathological features in familial AD (Arber et al., 2021; Kwart et al., 2019; Ng et al., 2022; Penney et al., 2020; Yang et al., 2017). Even though sporadic AD accounts for the vast majority of AD cases (Masters et al., 2015), the complex genetic compositions have made it much more

* Corresponding authors.
E-mail addresses: zhenyan@buffalo.edu (Z. Yan), jianfeng@buffalo.edu (J. Feng).
[1] These authors contributed equally to this work.

https://doi.org/10.1016/j.nbd.2026.107345
Received 16 December 2025; Received in revised form 25 February 2026; Accepted 4 March 2026
Available online 5 March 2026

challenging to use iPSC-derived neurons to study sAD (Cohen and Sonntag, 2024). Nevertheless, our recent study in iPSC-derived cortical neurons from sAD patients confirmed a consistent and significant increase in SGK1 expression (Saleem et al., 2025). In the present study, we focused on mature cortical neurons differentiated from iPSCs of four sAD patients and four healthy controls to identify electrophysiological changes, which may underlie neuronal communication deficits in AD patients. We found that cortical neurons derived from sAD patients exhibited significant reductions in voltage-gated Na^+ currents, evoked action potential (AP) amplitudes, and frequencies of spontaneous excitatory postsynaptic currents (sEPSCs) and spontaneous action potentials (APs). Notably, all these defects were rescued by SGK1 inhibition, which had negligible influences on control neurons.

2. Results

2.1. Decreased voltage-gated Na^+ currents in sAD cortical neurons

We differentiated 8 lines of iPSCs derived from 4 sAD and 4 control subjects to cortical neurons using the method that we developed recently (Jiang et al., 2025; Saleem et al., 2025). Information about the 8 subjects, including their *APOE* genotypes, is listed in Table 1. At day 100 or more of differentiation, most cells with neuronal morphology showed robust MAP2 expression with extensive neuronal processes in both control and sAD group (Fig. 1A). In addition, synaptic formations were similarly observed in control and sAD neurons as evidenced by the juxtaposition of the presynaptic protein synaptophysin and the postsynaptic protein GluR1 (Fig. 1B). Indeed, typical mature neuronal morphology can be visually identified under a phase contrast microscope (Fig. 1C), which allows us to perform electrophysiological studies on these neurons. No significant difference was found between control and sAD neurons in cell capacitance (AD vs. CON, $p = 0.8432$) (Fig. 1D) and resting membrane potential (RMP) (AD vs. CON, $p = 0.6094$) (Fig. 1E). Given the critical roles of Na^+ dysregulation in AD mouse models (Kim et al., 2007) and AD patients (Faraco et al., 2019; Mohan, et al., 2020; Vitvitsky et al., 2012), we performed whole-cell voltage clamp recordings to evaluate the flow of Na^+ and K^+. In both control and sAD neurons of mature neuronal morphology, whole-cell voltage-gated Na^+ and K^+ currents could be successfully elicited (Fig. 1F). However, the inward Na^+ currents in sAD patients were significantly smaller, as shown in the I-V curves (Fig. 1G) and the quantifications of currents elicited at −20 mV (AD vs. CON, $p = 0.0030$) (Fig. 1H). In contrast, there was no significant difference between control and sAD neurons in outward K^+ currents elicited at +40 mV (AD vs. CON, $p = 0.1619$) (Fig. 1I-J).

2.2. Reduced action potential amplitudes in sAD cortical neurons

Considering the critical role of Na^+ influx in eliciting an action potential, we next examined evoked action potentials (eAPs) in the cortical neurons from control and sAD patients using whole-cell current clamp recordings. With a minimum current injection to hold the membrane potential at −60 mV, neurons from both control and sporadic AD patients fired mature APs in response to 20 pA current injections (Fig. 2A). The average eAP frequency in response to the 20 pA current injection had no significant difference between control and sAD neurons (AD vs. CON, $p = 0.2564$) (Fig. 2B). However, sAD neurons exhibited a modest but significant reduction in the amplitude of eAP (AD vs. CON, $p = 0.0166$) (Fig. 2C) and a commensurate decrease in eAP overshoots (AD vs. CON, $p = 0.0274$) (Fig. 2D). There were no significant changes in the threshold (AD vs. CON, $p = 0.3522$) (Fig. 2E) and half-width (AD vs. CON, $p = 0.7210$) (Fig. 2F) of eAPs between normal and sAD neurons.

2.3. Attenuated sEPSC and sAP frequencies in sAD cortical neurons

Given the key role of excitatory synaptic transmission in cognitive functions (Paula-Lima et al., 2013), we examined the activities of the neuronal network by recording spontaneous excitatory postsynaptic currents (sEPSCs) under the voltage-clamp mode. There was a drastic decrease of sEPSC frequency in sAD cortical neurons (AD vs. CON, $p = 0.0040$) (Fig. 3A-B), but no significant change in sEPSC amplitude (AD vs. CON, $p = 0.3728$) (Fig. 3C). To substantiate these results, we recorded spontaneous action potential (sAP) under the current-clamp mode (Fig. 3D). There was a significant decrease in sAP frequency in sAD cortical neurons (AD vs. CON, $p = 0.0045$) (Fig. 3E) without an appreciable change in sAP amplitude (AD vs. CON, $p = 0.9543$) (Fig. 3F).

2.4. SGK1 inhibition increases Na^+ and K^+ currents in sAD neurons

The coordinated reductions in voltage-gated Na^+ current (Fig. 1), eAP amplitude (Fig. 2), and frequencies of sEPSC and sAP (Fig. 3) led us to examine the role of SGK1, whose elevated levels in AD postmortem patient brains (Cao et al., 2020) and iPSC-derived cortical neurons (Saleem et al., 2025) were linked to deficits in synaptic transmission and cognitive functions in P301S Tau transgenic mice (Cao et al., 2020). Control and sAD cortical neurons were treated with the selective SGK1 inhibitor (SGK1i) GSK650394 (100 nM for 72 h) or DMSO before recording whole-cell voltage-gated Na^+ and K^+ currents (Fig. 4A). SGK1i significantly increased voltage-gated Na^+ currents in sAD neurons (AD+SGK1i vs. AD+DMSO, $p = 0.0201$) but not in control neurons (CON+SGK1i vs. CON+DMSO, $p > 0.9999$) (Fig. 4B-C). In addition, SGK1 inhibition produced similar increases in voltage-gated K^+ currents in sAD and control neurons, although statistical significance was reached only in sAD (AD+SGK1i vs. AD+DMSO, $p = 0.0428$), but not control neurons (CON+SGK1i vs. CON+DMSO, $p = 0.6564$) (Fig. 4D-E).

2.5. SGK1 inhibition restores eAP amplitudes in sAD neurons

Next, we examined evoked action potentials (eAPs) elicited by an injection of 20 pA currents in control and sAD cortical neurons treated with GSK650394 (100 nM for 72 h) or DMSO (Fig. 5A). The SGK1 inhibitor had no significant impact on eAP frequency in sAD (AD+SGK1i vs. AD+DMSO, $p = 0.8517$) or control neurons (CON+SGK1i vs. CON+DMSO, $p > 0.9999$) (Fig. 5B). It significantly increased the amplitude of eAP in sAD (AD+SGK1i vs. AD+DMSO, $p = 0.0124$), but not control neurons (CON+SGK1i vs. CON+DMSO, $p > 0.9999$) (Fig. 5C). A commensurate increase of eAP overshoot was induced by SGK1i in sAD (AD+SGK1i vs. AD+DMSO, $p = 0.0173$), but not control neurons (CON+SGK1i vs. CON+DMSO, $p > 0.9999$) (Fig. 5D). SGK1 inhibition had no appreciable effects on eAP threshold (AD+SGK1i vs. AD+DMSO: $p = 0.7484$, CON+SGK1i vs. CON+DMSO: $p > 0.9999$) (Fig. 5E) and half-width (AD+SGK1i vs. AD+DMSO: $p = 0.3898$,

Table 1
APOE genotypes of iPSCs used in the study.

	Control				AD			
ID	CW70305	CW70256	CW70344	CW50040	CW50018	CW50024	CW50158	CW50170
Sex	F	F	M	M	F	M	M	F
Race	Caucasian							
Age at Sampling	56	61	62	63	58	63	63	64
APOE Genotype	*ε2/ε3*	*ε3/ε3*	*ε3/ε4*	*ε2/ε3*	*ε3/ε3*	*ε3/ε3*	*ε2/ε3*	*ε3/ε4*

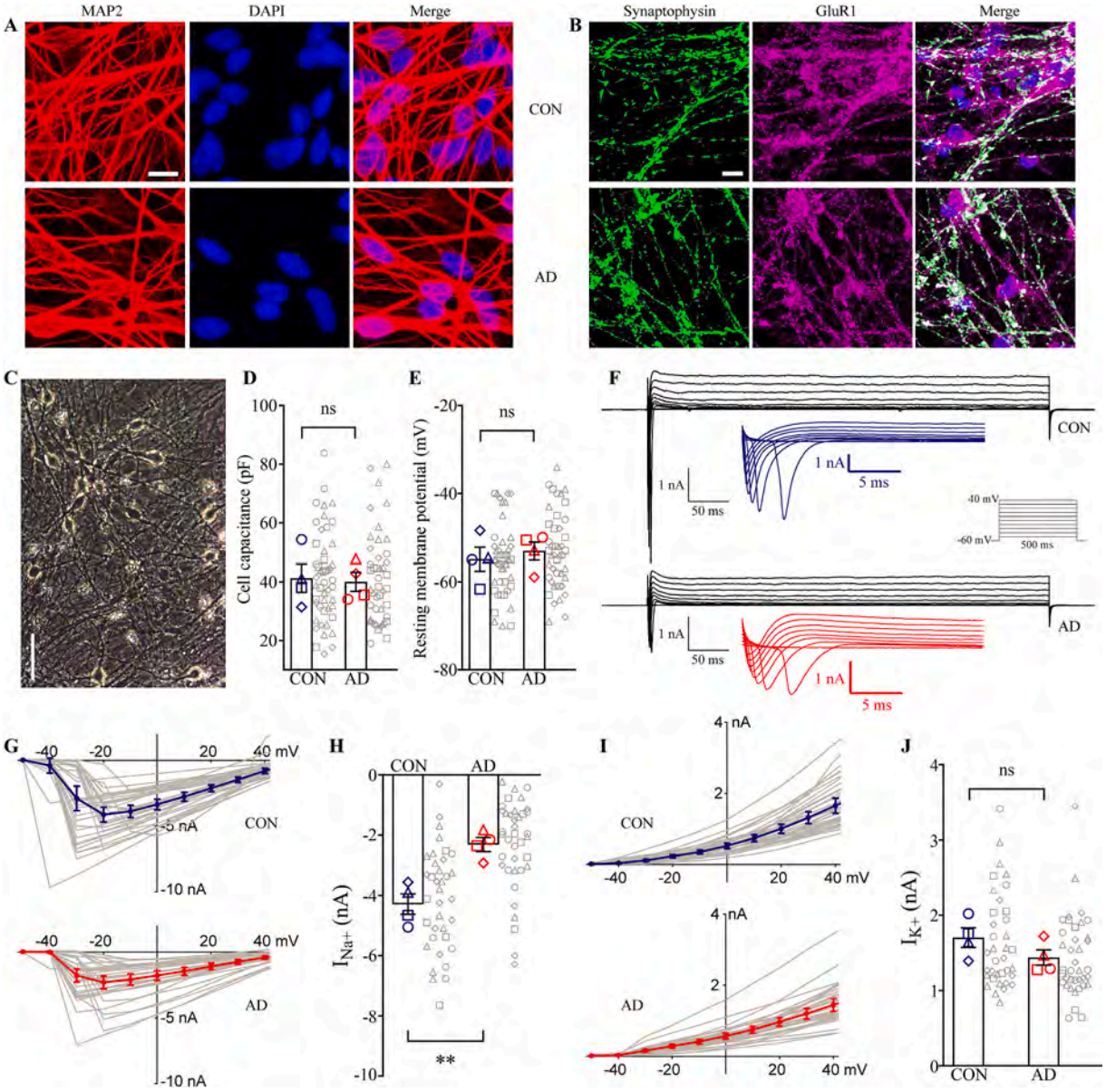

Fig. 1. Diminished voltage-gated Na^+ currents in AD cortical neurons. (A-B) Human iPSC-derived cortical neurons from healthy control (top) and sAD patients (bottom) at day 110 were costained as indicated. Scale bar, 10 μm. (C) A representative phase contrast image of iPSC-derived human cortical neurons on day 100. Scale bar, 30 μm. (D) Cell capacitance of control and AD neurons. CON: $n = 4$ (8, 10, 19, 11 cells / line); AD: n = 4 (10, 11, 15, 9 cells / line); $p = 0.8432$. (E) Resting membrane potential of control and AD neurons. CON: n = 4 (8, 9, 19, 11 cells / line); AD: n = 4 (10, 11, 14, 9 cells / line); $p = 0.6094$. (F) Representative voltage-gated Na^+ and K^+ currents (black) induced by depolarizing voltage steps (grey) in control (top) and AD neurons (bottom). Insets, enlarged traces for control (blue) and AD (red) neurons. (G) Averaged I-V curves (colored) for Na^+ currents in individual neurons (grey) derived from control subjects (top) and AD patients (bottom). (H) Peak Na^+ currents evoked at −20 mV in control and AD neurons. CON: n = 4 (10, 6, 14, 6 cells / line); AD: n = 4 (10, 6, 10, 12 cells / line); $p = 0.0030$. (I) Averaged I-V curves (colored) for fast K^+ currents in individual neurons (grey) derived from control subjects (top) and AD patients (bottom). (J) Peak fast K^+ currents evoked at +40 mV in control and AD neurons CON: n = 4 (10, 6, 14, 6 cells / line); AD: n = 4 (10, 6, 10, 12 cells / line); $p = 0.1619$. ** $p < 0.01$, unpaired two-tailed student's *t*-test; error bars, standard error of measurement; ns, non-significant ($p > 0.05$). n lists the number of human iPSC lines per group, with the number of cortical neurons from each line of CON (CW70305, CW70256, CW70344, CW50040) or AD group (CW50018, CW50024, CW50158, CW50170) listed in order inside the brackets. In all figures, data from different lines in control or AD groups were coded with distinct shapes to show variations of neurons within each line: rhombus for CON (CW70305) or AD group (CW50018), square for CON (CW70256) or AD group (CW50024), triangle for CON (CW70344) or AD group (CW50158) and circle for CON (CW50040) or AD group (CW50170). (For interpretation of the references to colour in this figure legend, the reader is referred to the web version of this article.)

CON+SGK1i vs. CON+DMSO: $p = 0.6082$) (Fig. 5F) in sAD or control neurons.

2.6. *SGK1 inhibition rescues reduced frequencies of sEPSC and sAP in sAD neurons*

Effects of GSK650394 (100 nM for 72 h) or DMSO on sEPSCs in control and sAD cortical neurons were compared (Fig. 6A). The SGK1 inhibitor markedly increased sEPSC frequency in sAD (AD+SGK1i vs. AD+DMSO, $p = 0.0324$) but not control neurons (CON+SGK1i vs. CON+DMSO, $p > 0.9999$) (Fig. 6B), without changing sEPSC amplitude (AD+SGK1i vs. AD+DMSO: $p = 0.9724$, CON+SGK1i vs. CON+DMSO: $p = 0.9996$) (Fig. 6C). We also examined spontaneous action potentials (sAP) in control and sAD cortical neurons treated with SGK1i or DMSO

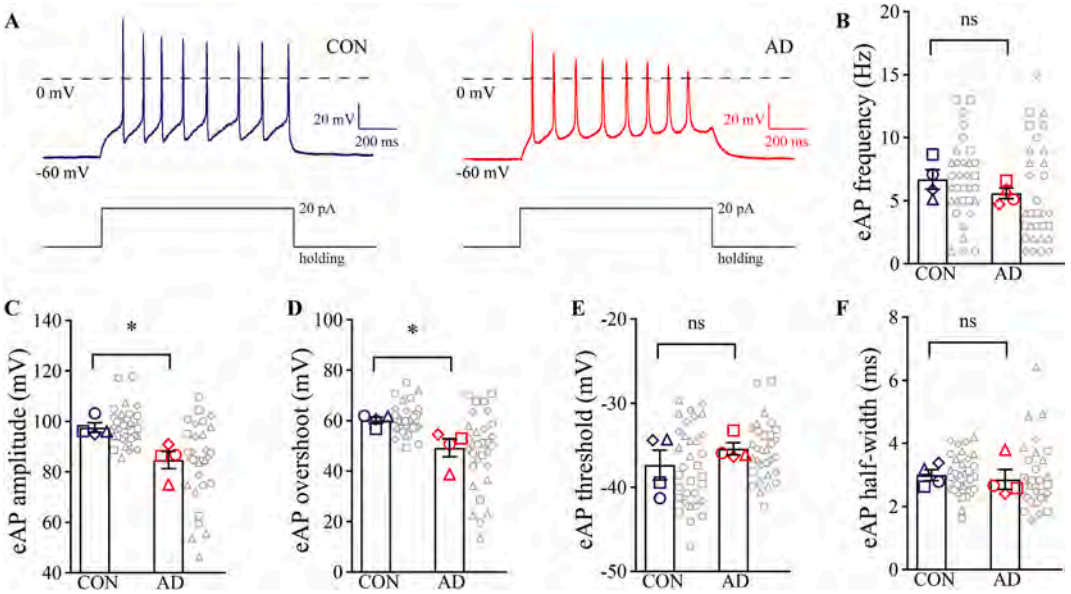

Fig. 2. Reduced action potential amplitudes in AD cortical neurons. (A) Representative traces of evoked action potentials (eAPs) elicited by 20 pA current injection (grey) from control (blue) and AD neurons (red), with RMP held at -60 mV. (B) AP frequencies in response to this stimulation in control and AD neurons ($p = 0.2564$). (C-F) The first AP in the burst was used for spike shape analysis. AP shape analysis for peak amplitudes ($p = 0.0166$) (C), overshoots ($p = 0.0274$) (D), threshold ($p = 0.3522$) (E), and half-width ($p = 0.7210$) (F). CON: n = 4 (8, 6, 9, 10 cells / line); AD: n = 4 (7, 5, 10, 9 cells / line). *$p < 0.05$,unpaired two-tailed student's t-test; error bars, standard error of measurement; ns, non-significant ($p > 0.05$), n lists the number of human iPSC lines per group, with the number of cortical neurons from each line of CON (CW70305, CW70256, CW70344, CW50040) or AD group (CW50018, CW50024, CW50158, CW50170) listed in order inside the brackets. (For interpretation of the references to colour in this figure legend, the reader is referred to the web version of this article.)

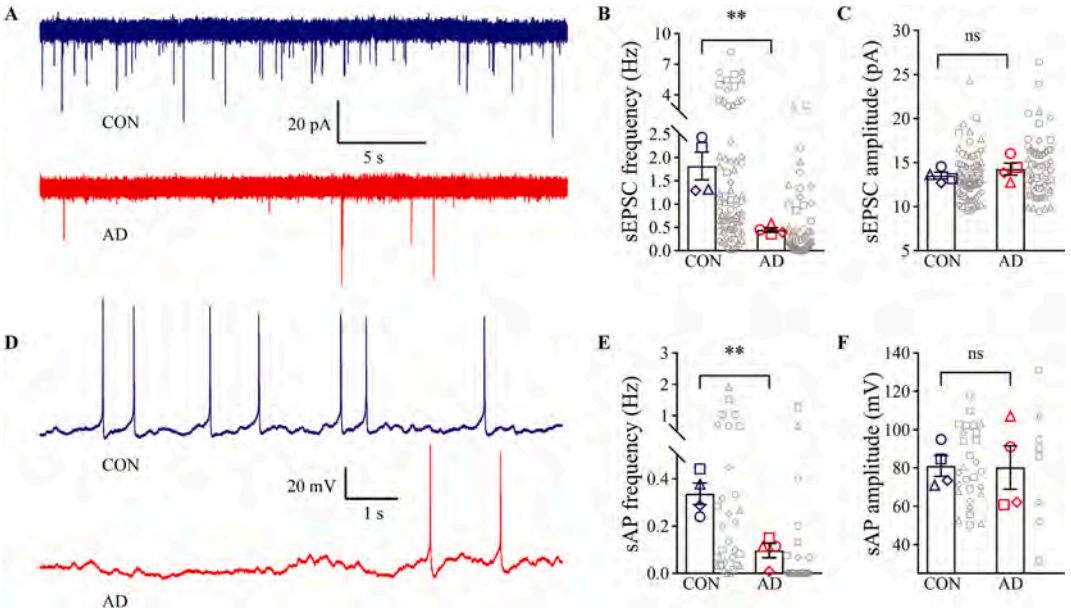

Fig. 3. Decreased frequencies of sEPSC and sAP in AD neurons. (A) Representative traces of spontaneous excitatory postsynaptic currents (sEPSC) recorded at -60 mV in control (blue) and AD neurons (red). (B, C) sEPSC frequency ($p = 0.0040$) (B) and amplitude ($p = 0.3728$) (C) in control and AD neurons. CON: n = 4 (15, 14, 33, 11 cells / line); AD: n = 4 (16, 19, 13, 18 cells / line) for (B), CON: n = 4 (15, 14, 33, 11 cells / line); AD: n = 4 (16, 14, 10, 17 cells / line) for (C). (D) Representative traces of spontaneous Action Potentials (sAP) recorded from control (blue) and AD neurons (red). (E, F) sAP frequency ($p = 0.0045$) (E) and amplitude ($p = 0.9543$) (F) in control and AD neurons. CON: n = 4 (8, 11, 6, 5 cells / line); AD: n = 4 (8, 9, 6, 7 cells / line) for (E), CON: n = 4 (8, 11, 5, 4 cells / line); AD: n = 4 (1, 2, 1, 4 cells / line) for (F). **$p < 0.01$, unpaired two-tailed student's t-test; error bars, standard error of measurement; ns, non-significant ($p > 0.05$), n lists the number of human iPSC lines per group, with the number of cortical neurons from each line of CON (CW70305, CW70256, CW70344, CW50040) or AD group (CW50018, CW50024, CW50158, CW50170) listed in order inside the brackets. (For interpretation of the references to colour in this figure legend, the reader is referred to the web version of this article.)

(Fig. 6D). SGK1 inhibition tended to selectively increase sAP frequency in sAD but not control neurons (AD+SGK1i vs. AD+DMSO: $p = 0.0108$, CON+SGK1i vs. CON+DMSO: $p = 0.4076$; two-tailed Student's *t*-tests; AD+SGK1i vs. AD+DMSO: $p = 0.2975$, CON+SGK1i vs. CON+DMSO: $p = 0.4396$; two-way ANOVA followed by Bonferroni's multiple comparisons.) (Fig. 6E).

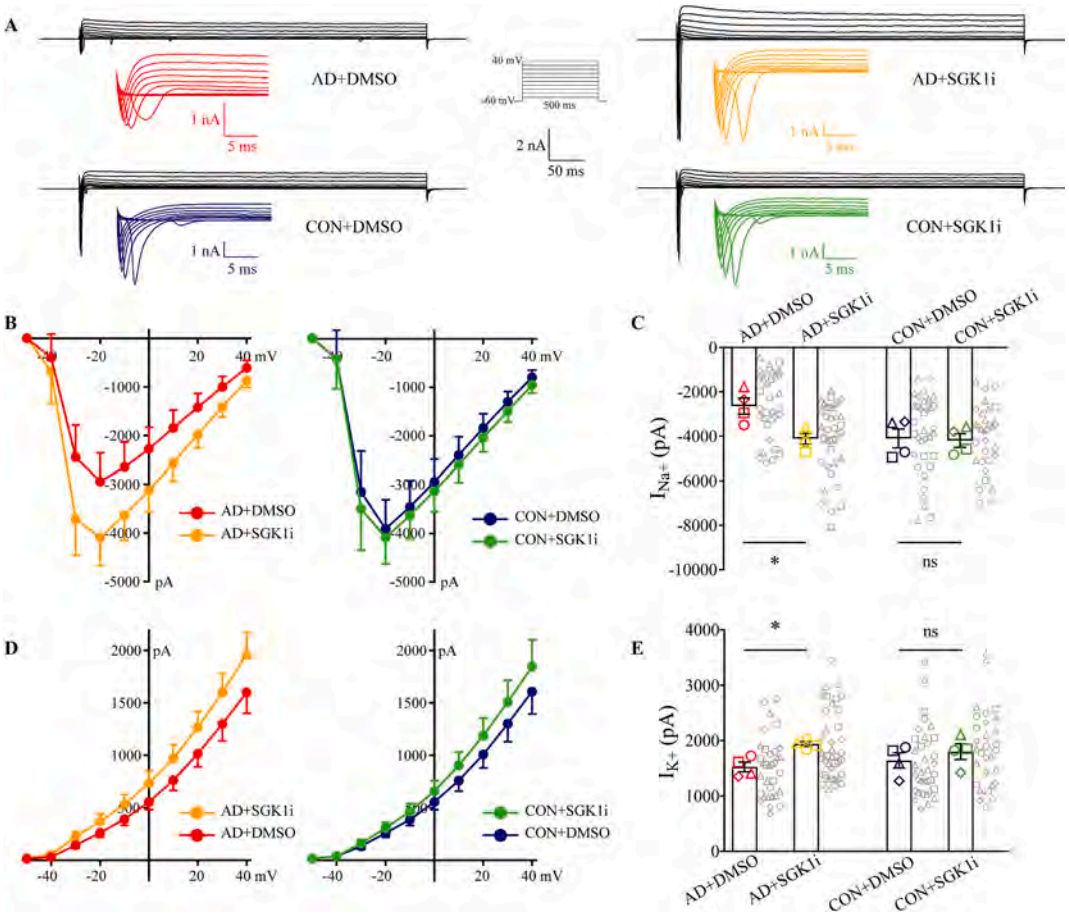

Fig. 4. SGK1 inhibition restores voltage-gated Na^+ and K^+ currents in AD neurons without affecting control neurons. (A) Representative traces of voltage-gated Na^+ and K^+ currents (black traces and scale bar) induced by depolarizing voltage steps (grey inset) in AD or control neurons treated with DMSO or the SGK1 inhibitor (SGK1i) GSK650394 (100 nM, 72 h). Colour insets, enlarged traces for each condition coded with colour. (B, C) Averaged I-V curves for voltage-gated Na^+ currents (B) and peak Na^+ currents at −20 mV in AD ($p = 0.0201$) or control neurons ($p > 0.9999$) treated with DMSO or SGK1i (C). (D, E) Averaged I-V curves for voltage-gated K^+ currents (D) and peak K^+ currents at +40 mV (E) in AD ($p = 0.0428$) or control neurons ($p = 0.6564$) treated with DMSO or SGK1i. * $p < 0.05$, two-way ANOVA followed by Bonferroni's multiple comparisons. AD+DMSO: n = 4 (6, 6, 12, 9 cells / line); AD+SGK1i: n = 4 (6, 8, 11, 14 cells / line); CON+DMSO: n = 4 (9, 6, 13, 7 cells / line); CON+SGK1i: n = 4 (7, 3, 12, 9 cells / line). n lists the number of human iPSC lines per group, with the number of cortical neurons from each line of CON (CW70305, CW70256, CW70344, CW50040) or AD group (CW50018, CW50024, CW50158, CW50170) listed in order inside the brackets.

3. Discussion

Using postmortem brain tissues (Cao et al., 2020) and iPSC-derived cortical neurons (Saleem et al., 2025) from sAD patients and the P301S human Tau transgenic mice (Cao et al., 2020), we have found that elevated SGK1 expression and activation contribute to tau hyperphosphorylation, microtubule destabilization, and cognitive impairment. The present study identified a series of coordinated electrophysiological defects in iPSC-derived cortical neurons from sAD patients. These findings may connect the elevation of cellular stress-induced kinase SGK1 to the memory and cognitive impairments observed in AD animal models. The reduction in voltage-gated Na^+ currents may contribute to the smaller amplitude of evoke AP, as less activation of voltage-gated Na^+ channels and unchanged voltage-gated K^+ currents would reduce the peak of AP. This should decrease the excitability of the sAD cortical neurons. Indeed, the frequencies of sEPSC and sAP were significantly reduced. The reduction of sEPSC frequency, but not amplitude, suggests a reduction in presynaptic glutamate release in sAD neurons. The reduced sAP frequency in sAD neurons may result from a combination of decreased excitatory input to the neuron and/or lower intrinsic excitability of the neuron. What is more remarkable is that not only these electrophysiological phenotypes were consistent with each other, but they were all rescued by SGK1 inhibition in sAD neurons. It suggests that SGK1 may activate a series of cellular events that target voltage-gated Na^+ channel and possibly other key components of synaptic integration and synaptic transmission to attenuate excitatory neurotransmission. Reduced neuronal excitability would lower metabolic demand on the neuron to generate ATP and maintain intracellular Ca^{2+} homeostasis, which produce oxidative stress in the cell (Chintaluri and Vogels, 2023; De La Rossa et al., 2022). Thus, SGK1 appears to function as a homeostatic regulator in response to cellular stress emanated from complex genetic factors in sAD neurons. It seems plausible that sAD neurons may attenuate neurotransmission to reduce cellular stress and enhance survival. Cognitive and memory impairments may be simply the system-level consequence of prioritizing neuronal survival at the expense of reducing synaptic transmission, before the accumulation of cellular stress eventually kills the diseased neurons.

Previous studies have shown the shift from hyper- to hypoexcitability in cortical networks as a hallmark of sAD, driven by the interplay of β-amyloid and tau pathologies that disrupt neuronal excitability, synaptic plasticity, and inhibitory circuits (Busche and Hyman, 2020; Phillips et al., 2023). Cortical hypoexcitability is observed in AD patients using transcranial magnetic stimulation (TMS)-electroencephalogram (EEG) (Ferreri et al., 2021) and magnetoencephalography (MEG) studies (Wiesman et al., 2022). Hypoexcitability of the dorsomedial prefrontal

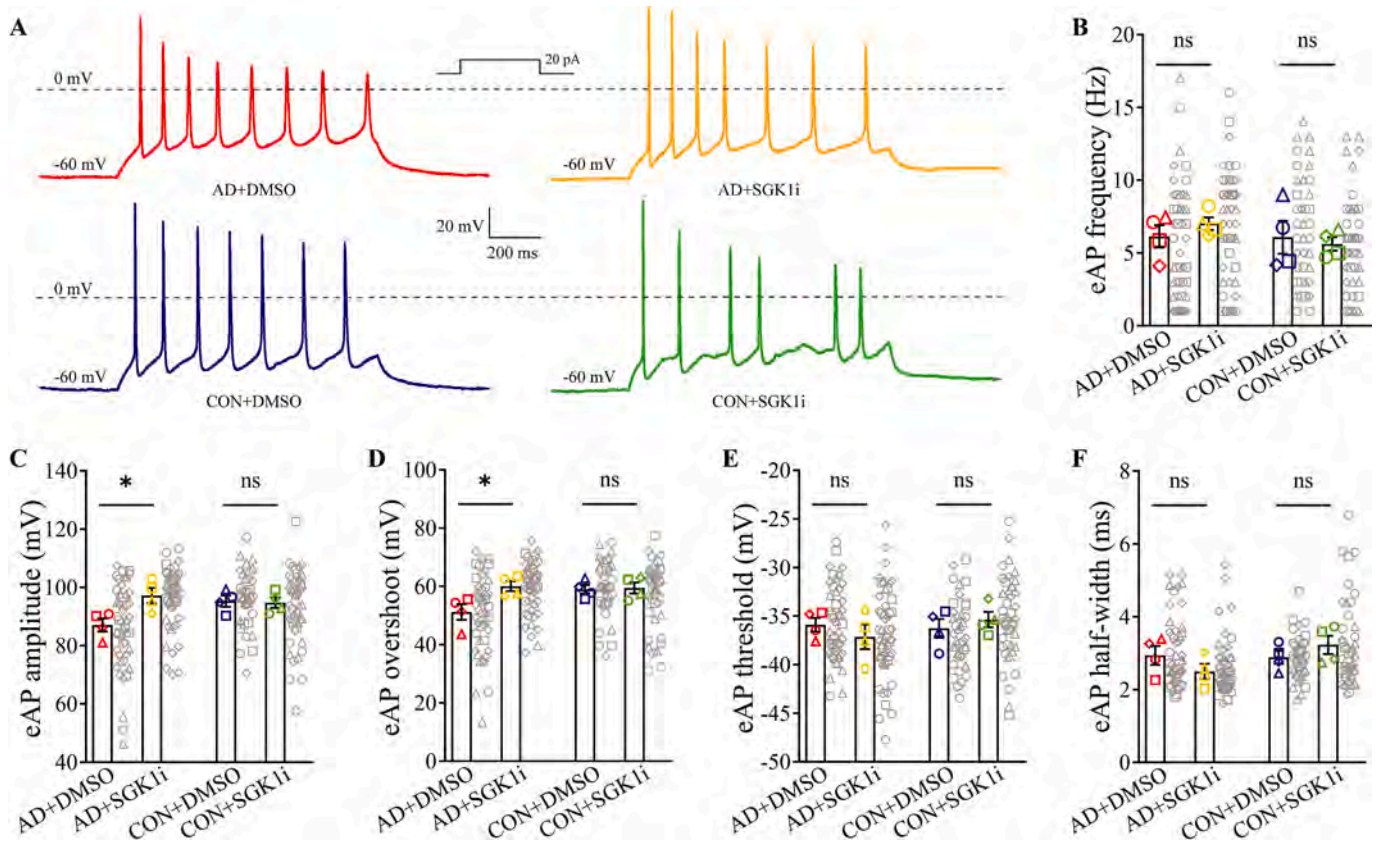

Fig. 5. SGK1 inhibition restores action potential amplitudes in AD neurons without affecting control neurons. (A) Representative traces of evoked action potentials (eAPs) elicited by 20 pA current injection (grey inset) in AD or control neurons treated with DMSO or the SGK1 inhibitor (SGK1i) GSK650394 (100 nM, 72 h). (B) Frequency of eAP for each condition (AD: $p = 0.8517$, control: $p > 0.9999$). (C-F) The first eAP in the burst were analyzed for amplitude (AD: $p = 0.0124$, control: $p > 0.9999$) (C), overshoot (AD: $p = 0.0173$, control: $p > 0.9999$) (D), threshold (AD: $p = 0.7484$, control: $p > 0.9999$) (E), and half-width (AD: $p = 0.3898$, control: $p = 0.6082$) (F). * $p < 0.05$, two-way ANOVA followed by Bonferroni's multiple comparisons. AD+DMSO: n = 4 (20, 8, 11, 8 cells / line); AD+SGK1i: n = 4 (20, 8, 9, 13 cells / line); CON+DMSO: n = 4 (6, 7, 13, 12 cells / line); CON+SGK1i: n = 4 (7, 4, 16, 18 cells / line). n lists the number of human iPSC lines per group, with the number of cortical neurons from each line of CON (CW70305, CW70256, CW70344, CW50040) or AD group (CW50018, CW50024, CW50158, CW50170) listed in order inside the brackets.

cortex underlies reduced empathy in the early-stage AD and other neurodegenerative dementias (Fischer et al., 2019,Giacomucci et al., 2022, Giacomucci et al., 2024,Phillips et al., 2023,Sturm et al., 2013). The present study has recapitulated neuronal hypoexcitability found in AD patient brains and validated the effectiveness of patient-specific iPSC-derived cortical neurons in dissecting the molecular and cellular mechanisms of sAD. Given that iPSC-derived neurons represent the fetal stage of development (Handel et al., 2016), our findings demonstrate that the intrinsic dysfunction of neurons and neuronal network can be captured in patient-specific cortical neurons in vitro decades before the onset of clinical symptoms and frank neuropathology. Multiple studies using iPSC-derived neurons from AD patients support this interpretation (Penney et al., 2020). Notably, longitudinal studies of subjects with dominantly inherited AD mutations have shown the development of cellular, pathological, and cognitive impairments 10 years or more before disease onset (Bateman et al., 2012). The different genetic composition of the sAD patients, when embodied in the iPSC-derived neurons, converged on the same set of coordinated electrophysiological phenotypes. The lack of in vivo organization of cells in this culture system strongly suggests the genetic basis of sAD.

Future studies are needed to understand how SGK1 is increased and activated in sAD cortical neurons. A variety of cellular stress, including oxidative stress, mitochondrial dysfunction, ER stress, misfolded protein stress, etc., are involved in the pathogenesis of AD (Butterfield and Halliwell, 2019; Salminen et al., 2009; Wang et al., 2020). It is critical to identify whether SGK1 is induced and activated by certain kinds of cellular stress in a specific manner. Another important follow-up study needs to uncover the SGK1 substrates responsible for the phenotypes that we observed in the present study. Transcriptomic and proteomic profiling of control and sAD cortical neurons may help reveal such targets and their post-translation modification states. By manipulating the identified targets, it is possible to characterize their involvement in the SGK1-dependent phenotypes. The identification of SGK1-dependent hypoexcitability in sAD cortical neurons in this study will pave the way to understanding molecular and cellular mechanisms of sAD through patient-specific iPSC-derived neurons. This fruitful strategy will facilitate the development of new therapies for Alzheimer's disease.

4. Material and methods

4.1. Sex as a biological variable

The study uses iPSCs derived from both male and female subjects, and similar findings are reported for both sexes.

4.2. Human iPSC lines and cell culture

We used iPSCs derived from 4 patients with sAD and 4 healthy control subjects. All 8 lines of iPSCs were made with non-integrating episomal vectors expressing Yamanaka factors by the Human Pluripotent Stem Cell Line Repository of California Institute for Regenerative Medicine (CIRM). Information about the 8 subjects, including their

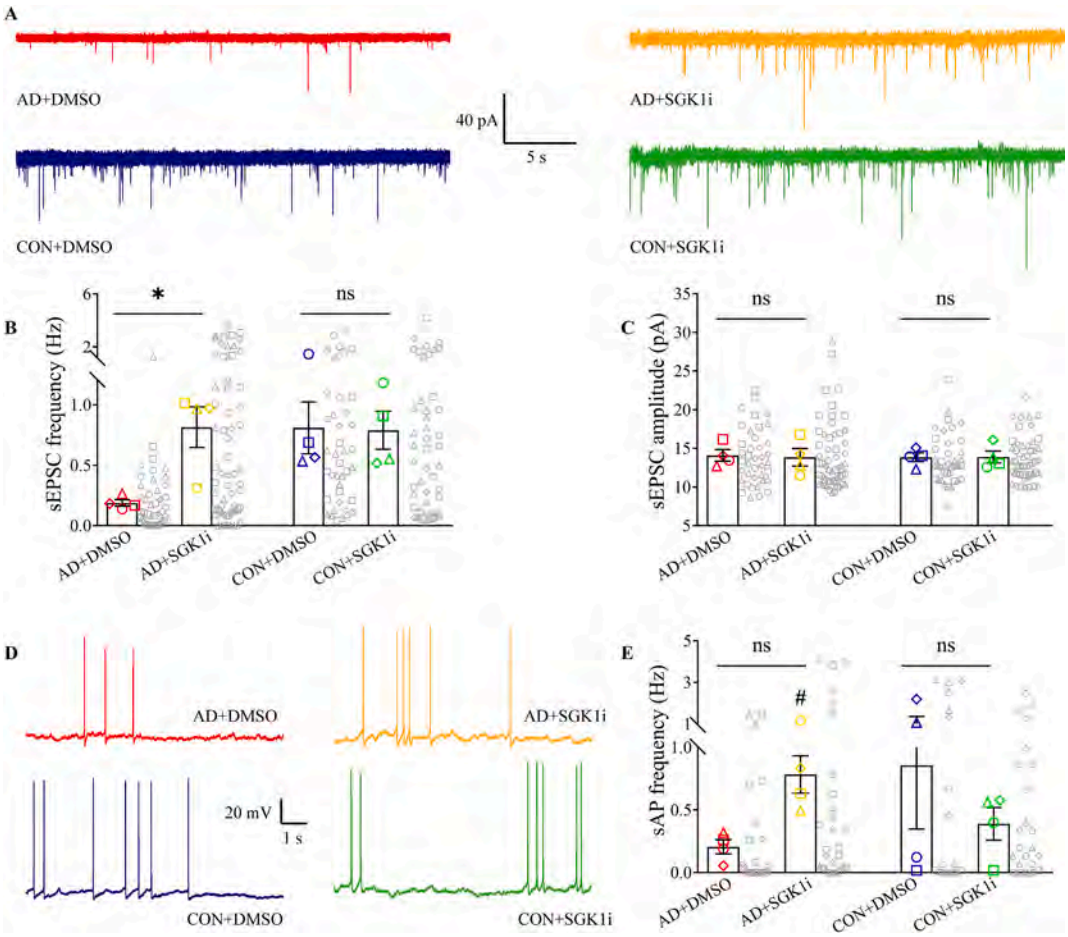

Fig. 6. SGK1 inhibition rescues sEPSC and sAP frequencies in AD neurons without affecting control neurons. (A) Representative traces of sEPSCs recorded at −60 mV in AD or control neurons treated with DMSO or the SGK1 inhibitor (SGK1i) GSK650394 (100 nM, 72 h). (B, C) Quantification of sEPSC frequency (sAD: $p = 0.0324$, control: $p > 0.9999$) (B) and amplitude (sAD: $p = 0.9724$, control: $p = 0.9996$) (C). AD+DMSO: n = 4 (8, 11, 14, 13 cells / line); AD+SGK1i: n = 4 (10, 18, 19, 15 cells / line); CON+DMSO: n = 4 (8, 10, 14, 8 cells / line); CON+SGK1i: n = 4 (8, 11, 20, 10 cells / line) for (B). AD+DMSO: n = 4 (8, 9, 12, 10 cells / line); AD+SGK1i: n = 4 (10, 18, 14, 13 cells / line); CON+DMSO: n = 4 (8, 10, 14, 8 cells / line); CON+SGK1i: n = 4 (8, 11, 20, 10 cells / line) for (C). (D, E) Representative traces (D) and frequency (sAD: $p = 0.2975$, control: $p = 0.4396$) (E) of sAPs recorded in AD or control neurons treated with DMSO or SGK1i. AD+DMSO: n = 4 (6, 10, 8, 6 cells / line); AD+SGK1i: n = 4 (2, 8, 13, 8 cells / line); CON+DMSO: n = 4 (2, 2, 10, 6 cells / line); CON+SGK1i: n = 4 (3, 1, 14, 8 cells / line). * $p < 0.05$, two-way ANOVA followed by Bonferroni's multiple comparisons. $^{\#}p < 0.05$, unpaired two-tailed student's t-test in E (sAD: $p = 0.0108$, control: $p = 0.4076$). n lists the number of human iPSC lines per group, with the number of cortical neurons from each line of CON (CW70305, CW70256, CW70344, CW50040) or AD group (CW50018, CW50024, CW50158, CW50170) listed in order inside the brackets.

APOE genotypes, is in Table 1. Human iPSCs were cultured on gamma-irradiated CF-1 mouse embryonic fibroblasts in a medium containing DMEM/F12, 20% knockout serum replacement, 0.1 mM β-mercaptoethanol, 1× NEAA, 1× L-glutamine, and 4–8 ng/ml FGF2. It is critical to maintain iPSCs on MEF because feeder-free cultures accumulate abnormal cells that have gained genomic damages (Stavish et al., 2024). The medium was changed daily. The cultures were passaged every 4–6 days at a ratio of 1:6 using dispase (1 mg/ml). All cell cultures were routinely checked by PCR to ensure the lack of Mycoplasma (Zhang et al., 2021).

4.3. APOE genotyping

Genomic DNA was isolated from the 8 lines of iPSCs using a QIAamp DNA mini-kit (Qiagen 51306). Two regions of the *APOE* exon 4 spanning the *ε2/ε3/ε4*-defining SNPs at codons 112 (rs429358) and 158 (rs7412) were amplified by PCR using the following primers: C112 forward: ACGGCTGTCCAAGGAGCTG, C112 reverse: AGCTTGCGCAGGTGGGA; C158 forward: GGACATGGAGGACGTGTG, C158 reverse GTACACTGCCAGGCGCTTC. PCR using the Phusion High-Fidelity PCR Kit (Thermo Scientific F-553S) was conducted under the following conditions: initial denaturation at 98 °C for 30 s, followed by 40 cycles of 98 °C for 10 s, 60 °C for 20 s, and 72 °C for 25 s, with a final extension at 72 °C for 2 min. PCR products were purified using the QIAquick Gel Extraction Kit (Qiagen 28704) and Sanger-sequenced using the forward PCR primer. *APOE* genotype was also determined by qPCR (Zhong et al., 2016). Genomic DNA was amplified with *ε2*, *ε3* or *ε4* primers separately with TaqPath ProAmp Master Mix and *APOE* TaqMan MGB probe tagged with FAM fluorescence reporter (both from Applied Biosystems). The qPCR was performed on CFX Duet RT-PCR System (BioRad) under the following conditions: pre-read at 60 °C for 30 s, denaturation at 95 °C for 5 min, followed by 40 cycles of 95 °C for 15 s and 64 °C for 60 s. The FAM signal was read at the end of each cycle.

4.4. Differentiation of human iPSCs to mature cortical neurons

The human iPSCs were differentiated into cortical neurons as previously described (Jiang et al., 2025). Briefly, iPSCs were dissociated with dispase to generate embryoid bodies (EBs), which were cultured in suspension in a 1:1 mixture of DMEM/F12 and Neurobasal media with 1× N2 supplement, 0.5× B27 supplement without vitamin A, 1× NEAA, ascorbic acid (0.2 mM), SB431542 (10 μM, days 0–6), dorsomorphin

dihydrochloride (5 μM, days 0–6), XAV939 (2.5 μM, days 0–10) and Cyclopamine (3.5 μM, days 0–10). On day 6, the EBs were plated on Matrigel-coated plates and cultured in the same media without SB431542 and dorsomorphin, with the medium changed every other day. On day 12, specified dorsal forebrain neuroepithelial cells in rosettes were dissociated into single cells with 1 unit/ml Accutase at 37 °C for 5 min and plated onto polyornithine/Matrigel-coated plates at a density of 5000–10,000 cells/cm^2 in a 1:1 medium of DMEM/F12 and Neurobasal that contained with 1× N2, 0.5× B27 without vitamin A, 1× NEAA and ascorbic acid (0.2 mM). The ROCK inhibitor Y27632 (20 μM) was added during the first 24 h. On day 18, cells were dissociated and plated onto polyornithine/Matrigel-coated glass coverslips in the Neurobasal medium that contained 1× B27 without vitamin A, Brain-derived Neurotrophic Factor (BDNF) (20 ng/ml), Glial cell line-derived Neurotrophic Factor (GDNF) (20 ng/ml), dibutyryl-cAMP (dcAMP) (0.25 mM) and DAPT (1 μM). Half of the medium was changed every other day. All neurons differentiated were maintained for at least 100 days before electrophysiological recordings.

4.5. Immunofluorescence and confocal imaging

Cortical neurons differentiated for 110 days from normal subjects and sAD patients were fixed with 4% paraformaldehyde for 15 min at 37 °C. Fixed neurons were washed twice with PBS and then permeabilized and quenched for 20 min in PBS with 0.2% saponin and 50 mM ammonium chloride at room temperature. After 3 washes with PBS, samples were incubated for 1 h in blocking buffer (PBS with 10% bovine serum albumin (BSA), 0.02% sodium azide (NaN3), and 0.02% saponin) at room temperature. Primary antibodies were diluted 1:5000 (chicken polyclonal anti-MAP2, Abcam Cat# ab5392), 1:1000 (rabbit polyclonal anti- synaptophysin, ThermoFisher Cat# PA1–1043), or 1:75 (mouse monoclonal anti-GluR1 (E6), Santa Cruz Cat# sc-13,152) in blocking buffer with reduced BSA (1%) and incubated with neurons overnight at 4 °C. After washing 4 times, fluorescent dye-conjugated secondary antibodies (11,000 dilution) were incubated with cells for 2 h at room temperature. Goat anti-chicken IgG secondary antibody, Alexa Fluor 647 (Cat# A-21449), Donkey anti-rabbit IgG secondary antibody, Alexa Fluor 647 (Cat# A-31573), and Donkey anti-mouse IgG secondary antibody, Alexa Fluor 594 (Cat# A-21203, all from ThermoFisher) were used. Cells were incubated with DAPI (300 nM) for 10 min to stain the nuclei. Confocal fluorescence images of neurons were captured using Leica TCS SP8 confocal microscope system with a 63× oil-immersion objective (NA 1.4).

4.6. Phase contrast imaging

The 40× representative image for hiPSC-derived cortical neurons at day 100 in culture medium were taken on the Olympus Microscope CKX41 with LCAch N 40× PhP as the objective lens, by INFINITY 2-1R digital CCD camera controlled by INFINITY ANALYZE Software v6.5 (Lumenera Corporation).

4.7. Solutions and chemicals

The extracellular solution for patch-clamp experiments contained 130 mM NaCl, 3 mM KCl, 1.2 mM $CaCl_2$, 1 mM $MgCl_2$, 10 mM HEPES-NaOH, and 10 mM glucose; the pH was adjusted to 7.3 with NaOH and the osmolarity was ~290 mOsm. The pipette solution contained 125 mM K-gluconate, 2 mM $MgCl_2$, 10 mM HEPES, 1 mM EGTA, 2 mM Na_2ATP, 0.4 mM Na_2GTP, and 5 mM Na_2-phosphocreatine; the pH was adjusted to 7.3 with KOH and the osmolarity was ~280 mOsm. The SGK1 inhibitor GSK650394 (Selleckchem) was prepared as a 100 mM stock solution in DMSO and diluted 1000× in neuronal culture medium.

4.8. Whole-cell patch-clamp recordings

Whole-cell patch-clamp was performed at room temperature (~20–25 °C). Neurons grown on glass coverslips were transferred from culture medium into the recording chamber on a Nikon Eclipse TE300 Nomarski DIC Phase Contrast Fluorescence Inverted Microscope. At 40× magnification, recordings of cells with mature neuronal morphology were obtained with an Axon Instruments 200B amplifier controlled and monitored by a PC running pClamp 10.0 with a DigiData 1440 A series interface (Axon instruments). In voltage-clamp mode, neurons held at −60 mV were depolarized by 500-ms pulses of voltage steps with a frequency of 0.1 Hz (−50 mV to +40 mV, in 10 mV increments) to evoke voltage-gated Na^+ and K^+ currents. In current-clamp mode, with membrane potentials kept at −60 mV with a steady holding current, current injections were given as 20 pA for 1 s (1-s) duration to evoke action potentials (eAPs). Using gap free recording modes, spontaneous action potentials (sAPs) were recorded in current-clamp mode without any current injection, while spontaneous excitatory postsynaptic currents (sEPSCs) were recorded at −60 mV in voltage-clamp mode. Recordings were low-pass filtered at 2 kHz, digitized and sampled at 20 kHz. To maintain quality and stability of the recordings, access resistance, cell capacitance, and membrane resistance were continuously monitored and recorded through a membrane test using the Clampex software.

4.9. Electrophysiology analysis

4.9.1. Voltage-gated Na^+ and K^+ currents

Immediately following each depolarization step, typically within a time window of a few milliseconds, Na^+ currents were measured as the difference between the minimum currents and the baseline, while the fast K^+ currents were measured as the difference between the maximum current and baseline. The Na^+ and K^+ current amplitudes were statistically analyzed at specific test potentials (−20 mV for Na^+ current and + 40 mV for K^+ current). These specific test potentials were chosen because they represent the physiological conditions of a healthy neuron (Tripathi et al., 2024). Cell capacitance was acquired through a membrane test using the Clampex software. As no difference was observed in cell capacitance of neurons from sporadic AD and controls (Fig. 1D), Na^+ and the fast K^+ currents in this study were not normalized by cell capacitance.

4.9.2. Evoked action potentials

The total number of action potentials elicited by the 1-s current injection of 20 pA above the steady holding current was counted as eAP frequency. Neurons that needed more than 50 pA current injections to be held at −60 mV were discarded from the analysis. The first AP in the burst was used for spike shape analysis. AP overshoots were calculated as the maximum membrane potential during a spike. AP thresholds were the membrane potential at which the slope of the depolarizing membrane potential increased drastically, resulting in a full action potential. AP amplitudes were calculated as the difference between the maximum membrane potential during a spike and the threshold. Action potential half-width was calculated as the duration of the action potential at the voltage halfway between threshold and the action potential peak.

4.9.3. Synaptic transmission and spontaneous action potentials

sEPSCs were measured in voltage-clamp mode in a blocker-free recording medium. The neurons were held at −60 mV and postsynaptic currents were recorded in the patched neuron for 120 s. Based on the signal-to-noise ratio of our recording system, sEPSC events with amplitudes smaller than 5 pA were excluded from analysis. sEPSC frequencies were measured as the total event number over a 120-s recording duration divided by 120. Spontaneous APs (sAPs) were measured in current-clamp mode in the same blocker-free recording medium soon after the cell membrane broke, and the patch became

stabilized. Without any current injection, neurons were recorded for 60 s. The resting membrane potential (RMP) was measured as the averaged baseline readings when no AP firing happens, while sAP frequency was measured as the total number of spontaneous APs captured during the 60-s recording period divided by 60. The sAP amplitude for each cell was measured from the AP that has the least interference from other APs in 60 s.

4.9.4. Data analysis software

For imaging data, all images were processed with Fiji. For electrophysiology data, all raw Axon Binary File Format (ABF) data files collected by pClamp 10.0 (Molecular Devices) were saved into ABF 1.8 integer format. Converted data were sequentially analyzed in Igor Pro 8.04 (WaveMetrics) with TaroTools toolbox (Taro Ishikawa, Jikei University School of Medicine, Japan).

4.10. Statistical analysis

No statistical method was used to predetermine sample sizes, but our sample sizes are similar to those reported in previous studies (Essayan-Perez and Sudhof, 2023; Ghatak et al., 2019; Harbom et al., 2019). Data was expressed as mean ± SEM, with a 95% confidence interval (CI) around the mean. For SGK1 inhibition treatment, coverslips from each line were randomly assigned into DMSO or SGK1i groups, and side-by-side patch clamp recordings were performed 72 h after treatment. The 8 lines of iPSCs were differentiated into cortical neurons in at least three independent rounds of differentiation. High-quality electrophysiological recordings of each line of neurons were pooled from these independent rounds of differentiation. The number of neurons recorded for each line is given in the figure legends. Statistical analysis showing data variations is reported in the results, figure legends, and Supplemental Table 1. For Figs. 1–3, statistical analysis was performed with unpaired two-tailed student's *t*-test using GraphPad Prism 10. Unless otherwise specified, for data in Figs. 4–6, statistical analysis was performed with two-way ANOVA followed by Bonferroni's multiple comparisons test using GraphPad Prism 10. Values for n, t, df, and p for two-tailed student's t-test, F (DFn, DFd) and adjusted *p* values for ANOVA, were summarized in Supplemental Table 1.

CRediT authorship contribution statement

J.F., Z.Y. and Z.J. conceived the project. J.F. and Z.J. wrote the manuscript with input from all other authors. Z.J. performed all electrophysiological, ICC and imaging experiments and analyses. K.S. and Z. J. differentiated iPSCs into human neurons. E.F. and L.L. performed *APOE* genotyping. Z.Y. and J.F. acquired funding, administrated and supervised the project, manuscript writing, review & editing.

Ethical approval

Mouse embryonic fibroblasts (MEF) production from mouse embryos is conducted with the approval of University at Buffalo Institutional Animal Care and Use Committee (IACUC ID: TR202300049). The use of unidentified human iPSCs from a public repository is not human subject research.

Funding

The work is supported by the National Institutes of Health grants NS113763 (JF) and AG079797 (JF and ZY).

Declaration of competing interest

The authors have declared that no competing interest exists.

Appendix A. Supplementary data

Supplementary data to this article can be found online at https://doi.org/10.1016/j.nbd.2026.107345.

Data availability

The authors confirm that all data of this study are included in the article.

References

Arber, C., Lovejoy, C., Harris, L., Willumsen, N., Alatza, A., Casey, J.M., Lines, G., Kerins, C., Mueller, A.K., Zetterberg, H., Hardy, J., Ryan, N.S., Fox, N.C., Lashley, T., Wray, S., 2021 Jan 12. Familial Alzheimer's disease mutations in PSEN1 Lead to premature human stem cell neurogenesis. Cell Rep. 34 (2), 108615. https://doi.org/10.1016/j.celrep.2020.108615.

Bateman, R.J., Xiong, C., Benzinger, T.L., Fagan, A.M., Goate, A., Fox, N.C., Marcus, D.S., Cairns, N.J., Xie, X., Blazey, T.M., Holtzman, D.M., Santacruz, A., Buckles, V., Oliver, A., Moulder, K., Aisen, P.S., Ghetti, B., Klunk, W.E., McDade, E., Dominantly Inherited Alzheimer N, et al., 2012 Aug 30. Clinical and biomarker changes in dominantly inherited Alzheimer's disease. N. Engl. J. Med. 367 (9), 795–804. https://doi.org/10.1056/NEJMoa1202753.

Busche, M.A., Hyman, B.T., 2020 Oct. Synergy between amyloid-beta and tau in Alzheimer's disease. Nat. Neurosci. 23 (10), 1183–1193. https://doi.org/10.1038/s41593-020-0687-6.

Butterfield, D.A., Halliwell, B., 2019 Mar. Oxidative stress, dysfunctional glucose metabolism and Alzheimer disease. Nat. Rev. Neurosci. 20 (3), 148–160. https://doi.org/10.1038/s41583-019-0132-6.

Cao, Q., Wang, W., Williams, J.B., Yang, F., Wang, Z.J., Yan, Z., 2020 Dec. Targeting histone K4 trimethylation for treatment of cognitive and synaptic deficits in mouse models of Alzheimer's disease. Sci. Adv. 6 (50). https://doi.org/10.1126/sciadv.abc8096.

Chao, C.C., Ma, Y.L., Lee, E.H., 2007 Jun 6. Protein kinase CK2 impairs spatial memory formation through differential cross talk with PI-3 kinase signaling: activation of Akt and inactivation of SGK1. J. Neurosci. 27 (23), 6243–6248. https://doi.org/10.1523/JNEUROSCI.1531-07.2007.

Chintaluri, C., Vogels, T.P., 2023 Nov 28. Metabolically regulated spiking could serve neuronal energy homeostasis and protect from reactive oxygen species. Proc. Natl. Acad. Sci. USA 120 (48), e2306525120. https://doi.org/10.1073/pnas.2306525120.

Cohen, B.M., Sonntag, K.C., 2024 Aug. Identifying the earliest-occurring clinically targetable precursors of late-onset Alzheimer's disease. EBioMedicine 106, 105238. https://doi.org/10.1016/j.ebiom.2024.105238.

Davoody, S., Asgari Taei, A., Khodabakhsh, P., Dargahi, L., 2024 Apr. mTOR signaling and Alzheimer's disease: what we know and where we are? CNS Neurosci. Ther. 30 (4), e14463. https://doi.org/10.1111/cns.14463.

De La Rossa, A., Laporte, M.H., Astori, S., Marissal, T., Montessuit, S., Sheshadri, P., Ramos-Fernandez, E., Mendez, P., Khani, A., Quairiaux, C., Taylor, E.B., Rutter, J., Nunes, J.M., Carleton, A., Duchen, M.R., Sandi, C., Martinou, J.C., 2022 Feb 21. Paradoxical neuronal hyperexcitability in a mouse model of mitochondrial pyruvate import deficiency. Elife 11. https://doi.org/10.7554/eLife.72595.

Di Cristofano, A., 2017. SGK1: the dark side of PI3K signaling. Curr. Top. Dev. Biol. 123, 49–71. https://doi.org/10.1016/bs.ctdb.2016.11.006.

Elahi, M., Motoi, Y., Shimonaka, S., Ishida, Y., Hioki, H., Takanashi, M., Ishiguro, K., Imai, Y., Hattori, N., 2021 Aug 28. High-fat diet-induced activation of SGK1 promotes Alzheimer's disease-associated tau pathology. Hum. Mol. Genet. 30 (18), 1693–1710. https://doi.org/10.1093/hmg/ddab115.

Essayan-Perez, S., Sudhof, T.C., 2023 Oct 18. Neuronal gamma-secretase regulates lipid metabolism, linking cholesterol to synaptic dysfunction in Alzheimer's disease. Neuron 111 (20), 3176–3194 e7. https://doi.org/10.1016/j.neuron.2023.07.005.

Faraco, G., Hochrainer, K., Segarra, S.G., Schaeffer, S., Santisteban, M.M., Menon, A., Jiang, H., Holtzman, D.M., Anrather, J., Iadecola, C., 2019 Oct. Dietary salt promotes cognitive impairment through tau phosphorylation. Nature 574 (7780), 686–690. https://doi.org/10.1038/s41586-019-1688-z.

Ferreri, F., Guerra, A., Vollero, L., Ponzo, D., Maatta, S., Kononen, M., Vecchio, F., Pasqualetti, P., Miraglia, F., Simonelli, I., Corbetta, M., Rossini, P.M., 2021. TMS-EEG biomarkers of amnestic mild cognitive impairment due to Alzheimer's disease: a proof-of-concept six years prospective study. Front. Aging Neurosci. 13, 737281. https://doi.org/10.3389/fnagi.2021.737281.

Fischer, A., Landeira-Fernandez, J., Sollero de Campos, F., Mograbi, D.C., 2019. Empathy in Alzheimer's disease: review of findings and proposed model. J. Alzheimer's Dis 69 (4), 921–933. https://doi.org/10.3233/JAD-180730.

Ghatak, S., Dolatabadi, N., Trudler, D., Zhang, X., Wu, Y., Mohata, M., Ambasudhan, R., Talantova, M., Lipton, S.A., 2019 Nov 29. Mechanisms of hyperexcitability in Alzheimer's disease hiPSC-derived neurons and cerebral organoids vs isogenic controls. Elife 8. https://doi.org/10.7554/eLife.50333.

Giacomucci, G., Galdo, G., Polito, C., Berti, V., Padiglioni, S., Mazzeo, S., Chiaro, E., De Cristofaro, M.T., Bagnoli, S., Nacmias, B., Sorbi, S., Bessi, V., 2022 Jun 25. Unravelling neural correlates of empathy deficits in subjective cognitive decline, mild cognitive impairment and Alzheimer's Disease. Behav. Brain Res. 428, 113893. https://doi.org/10.1016/j.bbr.2022.113893.

Giacomucci, G., Moschini, V., Piazzesi, D., Padiglioni, S., Caruso, C., Nuti, C., Munarin, A., Mazzeo, S., Galdo, G., Polito, C., Emiliani, F., Frigerio, D., Morinelli, C., Bagnoli, S., Ingannato, A., Nacmias, B., Sorbi, S., Berti, V., Bessi, V., 2024 Mar. Disentangling empathy impairment along Alzheimer's disease continuum: from subjective cognitive decline to Alzheimer's dementia. Cortex 172, 125–140. https://doi.org/10.1016/j.cortex.2023.12.009.

Handel, A.E., Chintawar, S., Lalic, T., Whiteley, E., Vowles, J., Giustacchini, A., Argoud, K., Sopp, P., Nakanishi, M., Bowden, R., Cowley, S., Newey, S., Akerman, C., Ponting, C.P., Cader, M.Z., 2016 Mar 1. Assessing similarity to primary tissue and cortical layer identity in induced pluripotent stem cell-derived cortical neurons through single-cell transcriptomics. Hum. Mol. Genet. 25 (5), 989–1000. https://doi.org/10.1093/hmg/ddv637.

Harbom, L.J., Rudisill, T.L., Michel, N., Litwa, K.A., Beenhakker, M.P., McConnell, M.J., 2019 Mar. The effect of rho kinase inhibition on morphological and electrophysiological maturity in iPSC-derived neurons. Cell Tissue Res. 375 (3), 641–654. https://doi.org/10.1007/s00441-018-2942-7.

Jiang, H., Xiao, Z., Saleem, K., Zhong, P., Li, L., Chhetri, G., Li, P., Jiang, Z., Yan, Z., Feng, J., 2025 Apr 23. Generation of human induced pluripotent stem cell-derived cortical neurons expressing the six tau isoforms. J. Alzheimer's Dis. https://doi.org/10.1177/13872877251334831, 13872877251334831.

Kim, D.Y., Carey, B.W., Wang, H., Ingano, L.A., Binshtok, A.M., Wertz, M.H., Pettingell, W.H., He, P., Lee, V.M., Woolf, C.J., Kovacs, D.M., 2007 Jul. BACE1 regulates voltage-gated sodium channels and neuronal activity. Nat. Cell Biol. 9 (7), 755–764. https://doi.org/10.1038/ncb1602.

Kwart, D., Gregg, A., Scheckel, C., Murphy, E.A., Paquet, D., Duffield, M., Fak, J., Olsen, O., Darnell, R.B., Tessier-Lavigne, M., 2019 Oct 23. A large panel of isogenic APP and PSEN1 mutant human iPSC neurons reveals shared endosomal abnormalities mediated by APP beta-CTFs, not Abeta. Neuron 104 (2), 256–270 e5. https://doi.org/10.1016/j.neuron.2019.07.010.

Kwon, O.C., Song, J.J., Yang, Y., Kim, S.H., Kim, J.Y., Seok, M.J., Hwang, I., Yu, J.W., Karmacharya, J., Maeng, H.J., Kim, J., Jho, E.H., Ko, S.Y., Son, H., Chang, M.Y., Lee, S.H., 2021 Apr 9. SGK1 inhibition in glia ameliorates pathologies and symptoms in Parkinson disease animal models. EMBO Mol. Med. 13 (4), e13076. https://doi.org/10.15252/emmm.202013076.

Lang, F., Strutz-Seebohm, N., Seebohm, G., Lang, U.E., 2010 Sep 15. Significance of SGK1 in the regulation of neuronal function. J. Physiol. 588 (Pt 18), 3349–3354. https://doi.org/10.1113/jphysiol.2010.190926.

Lang, F., Stournaras, C., Zacharopoulou, N., Voelkl, J., Alesutan, I., 2018 Dec 2. Serum- and glucocorticoid-inducible kinase 1 and the response to cell stress. Cell Stress. 3 (1), 1–8. https://doi.org/10.15698/cst2019.01.170.

Lang, F., Rajaxavier, J., Singh, Y., Brucker, S.Y., Salker, M.S., 2020. The enigmatic role of Serum & Glucocorticoid Inducible Kinase 1 in the endometrium. Front. Cell Dev. Biol. 8, 556543. https://doi.org/10.3389/fcell.2020.556543.

Lian, B., Liu, M., Lan, Z., Sun, T., Meng, Z., Chang, Q., Liu, Z., Zhang, J., Zhao, C., 2020 Apr 6. Hippocampal overexpression of SGK1 ameliorates spatial memory, rescues Aβ pathology and actin cytoskeleton polymerization in middle-aged APP/PS1 mice. Behav. Brain Res. 383, 112503. https://doi.org/10.1016/j.bbr.2020.112503.

Masters, C.L., Bateman, R., Blennow, K., Rowe, C.C., Sperling, R.A., Cummings, J.L., 2015 Oct 15. Alzheimer's disease. Nat. Rev. Dis. Primers 1, 15056. https://doi.org/10.1038/nrdp.2015.56.

Mathys, H., Davila-Velderrain, J., Peng, Z., Gao, F., Mohammadi, S., Young, J.Z., Menon, M., He, L., Abdurrob, F., Jiang, X., Martorell, A.J., Ransohoff, R.M., Hafler, B.P., Bennett, D.A., Kellis, M., Tsai, L.H., 2019 Jun. Single-cell transcriptomic analysis of Alzheimer's disease. Nature 570 (7761), 332–337. https://doi.org/10.1038/s41586-019-1195-2.

Mohan, D., Yap, K.H., Reidpath, D., Soh, Y.C., McGrattan, A., Stephan, B.C.M., Robinson, L., Chaiyakunapruk, N., Siervo, M., De PECt, 2020. Link between dietary sodium intake, cognitive function, and dementia risk in middle-aged and older adults: a systematic review. J. Alzheimer's Dis 76 (4), 1347–1373. https://doi.org/10.3233/JAD-191339.

Ng, B., Rowland, H.A., Wei, T., Arunasalam, K., Hayes, E.M., Koychev, I., Hedegaard, A., Ribe, E.M., Chan, D., Chessell, T., Ffytche, D., Gunn, R.N., Kocagoncu, E., Lawson, J., Malhotra, P.A., Ridha, B.H., Rowe, J.B., Thomas, A.J., Zamboni, G., Wade-Martins, R., et al., 2022. Neurons derived from individual early Alzheimer's disease patients reflect their clinical vulnerability. Brain Commun. 4 (6), fcac267. https://doi.org/10.1093/braincomms/fcac267.

Paula-Lima, A.C., Brito-Moreira, J., Ferreira, S.T., 2013 Jul. Deregulation of excitatory neurotransmission underlying synapse failure in Alzheimer's disease. J. Neurochem. 126 (2), 191–202. https://doi.org/10.1111/jnc.12304.

Penney, J., Ralvenius, W.T., Tsai, L.H., 2020 Jan. Modeling Alzheimer's disease with iPSC-derived brain cells. Mol. Psychiatry 25 (1), 148–167. https://doi.org/10.1038/s41380-019-0468-3.

Phillips, H.L., Dai, H., Choi, S.Y., Jansen-West, K., Zajicek, A.S., Daly, L., Petrucelli, L., Gao, F.B., Yao, W.D., 2023 Mar 15. Dorsomedial prefrontal hypoexcitability underlies lost empathy in frontotemporal dementia. Neuron 111 (6), 797–806 e6. https://doi.org/10.1016/j.neuron.2022.12.027.

Rollo, J., Crawford, J., Hardy, J., 2023 Jul 19. A dynamical systems approach for multiscale synthesis of Alzheimer's pathogenesis. Neuron 111 (14), 2126–2139. https://doi.org/10.1016/j.neuron.2023.04.018.

Saleem, K., Xiao, Z., Zhu, B., Ren, Y., Yan, Z., Feng, J., 2025. Elevated SGK1 increases Tau phosphorylation and microtubule instability in Alzheimer's patient-derived cortical neurons. Mol. Psychiatry. https://doi.org/10.1038/s41380-025-03225-4.

Salminen, A., Kauppinen, A., Suuronen, T., Kaarniranta, K., Ojala, J., 2009 Dec 26. ER stress in Alzheimer's disease: a novel neuronal trigger for inflammation and Alzheimer's pathology. J. Neuroinflammation 6, 41. https://doi.org/10.1186/1742-2094-6-41.

Schoenebeck, B., Bader, V., Zhu, X.R., Schmitz, B., Lubbert, H., Stichel, C.C., 2005 Oct. Sgk1, a cell survival response in neurodegenerative diseases. Mol. Cell. Neurosci. 30 (2), 249–264. https://doi.org/10.1016/j.mcn.2005.07.017.

Stavish, D., Price, C.J., Gelezauskaite, G., Alsehli, H., Leonhard, K.A., Taapken, S.M., McIntire, E.M., Laing, O., James, B.M., Riley, J.J., Zerbib, J., Baker, D., Harding, A. L., Jestice, L.H., Eleveld, T.F., Gillis, A.J.M., Hillenius, S., Looijenga, L.H.J., Gokhale, P.J., Barbaric, I., et al., 2024 Aug 13. Feeder-free culture of human pluripotent stem cells drives MDM4-mediated gain of chromosome 1q. Stem Cell Rep. 19 (8), 1217–1232. https://doi.org/10.1016/j.stemcr.2024.06.003.

Sturm, V.E., Yokoyama, J.S., Seeley, W.W., Kramer, J.H., Miller, B.L., Rankin, K.P., 2013 Jun 11. Heightened emotional contagion in mild cognitive impairment and Alzheimer's disease is associated with temporal lobe degeneration. Proc. Natl. Acad. Sci. USA 110 (24), 9944–9949. https://doi.org/10.1073/pnas.1301119110.

Talarico, C., Dattilo, V., D'Antona, L., Barone, A., Amodio, N., Belviso, S., Musumeci, F., Abbruzzese, C., Bianco, C., Trapasso, F., Schenone, S., Alcaro, S., Ortuso, F., Florio, T., Paggi, M.G., Perrotti, N., Amato, R., 2016 Mar 29. SI113, a SGK1 inhibitor, potentiates the effects of radiotherapy, modulates the response to oxidative stress and induces cytotoxic autophagy in human glioblastoma multiforme cells. Oncotarget 7 (13), 15868–15884. https://doi.org/10.18632/oncotarget.7520.

Tripathi, U., Rosh, I., Ben Ezer, R., Nayak, R., Hussein, Y., Choudhary, A., Djamus, J., Manole, A., Houlden, H., Gage, F.H., Stern, S., 2024 May 18. Upregulated ECM genes and increased synaptic activity in Parkinson's human DA neurons with PINK1/PRKN mutations. NPJ Parkinsons Dis. 10 (1), 103. https://doi.org/10.1038/s41531-024-00715-0.

Tsai, K.J., Chen, S.K., Ma, Y.L., Hsu, W.L., Lee, E.H., 2002 Mar 19. sgk, a primary glucocorticoid-induced gene, facilitates memory consolidation of spatial learning in rats. Proc. Natl. Acad. Sci. USA 99 (6), 3990–3995. https://doi.org/10.1073/pnas.062405399.

Vitvitsky, V.M., Garg, S.K., Keep, R.F., Albin, R.L., Banerjee, R., 2012 Nov. Na+ and K+ ion imbalances in Alzheimer's disease. Biochim. Biophys. Acta 1822 (11), 1671–1681. https://doi.org/10.1016/j.bbadis.2012.07.004.

Wang, W., Zhao, F., Ma, X., Perry, G., Zhu, X., 2020 May 29. Mitochondria dysfunction in the pathogenesis of Alzheimer's disease: recent advances. Mol. Neurodegener. 15 (1), 30. https://doi.org/10.1186/s13024-020-00376-6.

Wiesman, A.I., Murman, D.L., Losh, R.A., Schantell, M., Christopher-Hayes, N.J., Johnson, H.J., Willett, M.P., Wolfson, S.L., Losh, K.L., Johnson, C.M., May, P.E., Wilson, T.W., 2022 Jun 30. Spatially resolved neural slowing predicts impairment and amyloid burden in Alzheimer's disease. Brain 145 (6), 2177–2189. https://doi.org/10.1093/brain/awab430.

Yang, J., Zhao, H., Ma, Y., Shi, G., Song, J., Tang, Y., Li, S., Li, T., Liu, N., Tang, F., Gu, J., Zhang, L., Zhang, Z., Zhang, X., Jin, Y., Le, W., 2017 Jan 31. Early pathogenic event of Alzheimer's disease documented in iPSCs from patients with PSEN1 mutations. Oncotarget 8 (5), 7900–7913. https://doi.org/10.18632/oncotarget.13776.

Zhang, B., Li, H., Hu, Z., Jiang, H., Stablewski, A.B., Marzullo, B.J., Yergeau, D.A., Feng, J., 2021 Aug. Generation of mouse-human chimeric embryos. Nat. Protoc. 16 (8), 3954–3980. https://doi.org/10.1038/s41596-021-00565-7.

Zhong, L., Xie, Y.Z., Cao, T.T., Wang, Z., Wang, T., Li, X., Shen, R.C., Xu, H., Bu, G., Chen, X.F., 2016 Jan 12. A rapid and cost-effective method for genotyping apolipoprotein E gene polymorphism. Mol. Neurodegener. 11, 2. https://doi.org/10.1186/s13024-016-0069-4.